LETTERS
PUBLISHED ONLINE: 4 APRIL 2016 | DOI: 10.1038/NMAT4610
nature materials

Interfacial geometry dictates cancer cell tumorigenicity

Junmin Lee[1], Amr A. Abdeen[1], Kathryn L. Wycislo[2], Timothy M. Fan[3] and Kristopher A. Kilian[1]*

Within the heterogeneous architecture of tumour tissue there exists an elusive population of stem-like cells that are implicated in both recurrence and metastasis[1,2]. Here, by using engineered extracellular matrices, we show that geometric features at the perimeter of tumour tissue will prime a population of cells with a stem-cell-like phenotype. These cells show characteristics of cancer stem cells *in vitro*, as well as enhanced tumorigenicity in murine models of primary tumour growth and pulmonary metastases. We also show that interfacial geometry modulates cell shape, adhesion through integrin $\alpha_5\beta_1$, MAPK and STAT activity, and initiation of pluripotency signalling. Our results for several human cancer cell lines suggest that interfacial geometry triggers a general mechanism for the regulation of cancer-cell state. Similar to how a growing tumour can co-opt normal soluble signalling pathways[3], our findings demonstrate how cancer can also exploit geometry to orchestrate oncogenesis.

Cancer is a leading cause of death, primarily through the process of metastasis where malignant cells spread to distant organs[4]. It is believed that 'tumour initiating cells' or 'cancer stem cells' (herein referred to as CSCs) inherently possess the characteristics necessary for establishing metastases; however, within a tumour mass comprised of billions of cells, usually only a small percentage of cells exhibit a CSC phenotype[2]. This same population of cells is believed to be the root cause of recurrence after treatment, because most therapeutic regimens have not been optimized to target CSCs, and there have been multiple examples of CSCs being resistant to therapy[5]. Current evidence suggests wide-scale dynamic variation in the presence and function of CSCs across cancers and patients[6]. Deciphering the cues in the microenvironment that promote the CSC phenotype is a pressing need for understanding disease progression and developing therapeutics that can disrupt the processes involved for induction and survival of CSCs.

Emerging evidence suggests that tumour cells may show 'plasticity' in response to microenvironmental cues. For example, melanoma cells have been shown to adopt a tumorigenic, CSC-like state and form new tumours after transplantation[7]. An exciting recent report showed how soft fibrin gels can promote selected growth of tumorigenic melanoma cells[8], and further investigation demonstrated how the mechanical properties of the matrix can regulate Sox2 expression[9]. However, the canonical self-renewal transcription factors Oct4 and Nanog were not activated in these cells. The influence of matrix mechanics on cancer cell tumorigenicity has been demonstrated in several other cancers[10]. Taken together, these reports show that, in addition to the classical models underlying tumour heterogeneity, tumour cells may exhibit more plasticity than originally anticipated, and may be influenced through biophysical cues in the tumour microenvironment.

Substrate stiffness is known to modulate cell behaviour[11] and gene expression[12]. Furthermore, the geometric organization of cells in tissue places them into variable regions of mechanical stress[13], which can influence proliferation[14], migration[15], branching[16], stem cell characteristics[17], and cancer cell survival and invasiveness[18,19]. For example, Nelson and colleagues demonstrated how geometry can guide epithelial to mesenchymal transitions (EMT) through mechanical stress in micropatterned mammary epithelial cells[18]. In this letter we use soft hydrogel microengineering to pattern populations of tumour cells on two-dimensional (2D) and within three-dimensional (3D) hydrogels of variable stiffness, with combinations of perimeter geometric cues, to explore how biophysical parameters influence CSC characteristics and tumorigenicity (Fig. 1a).

We prepared hydrazine-modified polyacrylamide (PA) hydrogels of different elasticity (~1, 10, and 100 kPa) and used soft lithography to conjugate matrix proteins in various patterns with different sizes and shapes (Supplementary Fig. 1). As a model system we selected the murine B16 melanoma cell lines and used putative CSC molecular markers CD271, CD133 and ABCB5 (refs 20–22). We first measured these markers in B16 melanoma cells cultured for 1, 3 and 5 days on circular patterns of different matrix elasticity and pattern size (Supplementary Fig. 2). Expression of tumorigenic molecular markers strongly depended on culture duration (1–5 days) and colony size, with a maximum at the perimeter of circular islands ~3,000–100,000 μm^2. The stiffness of the underlying matrix did not exert a significant influence over the expression of CSC markers, thus we fixed the stiffness of our matrices at 10 kPa (Fig. 1b and Supplementary Fig. 3). Analysis of cell morphology at these perimeter features reveals that, with decreasing pattern size, individual cells occupy longer arcs along the pattern perimeter, with larger subtended arc angles on average. This correlates with higher ABCB5 expressions in these cells (Fig. 1c). For instance, an average cell on the perimeter of a 3,000 μm^2 pattern has an edge curvature ~2.2 times longer, with an angle of curvature ~12.7 times larger, and shows ~2.6 times higher ABCB5 expression than a cell on a 10,000 μm^2 pattern. Analysis of cell and nuclear shapes, proliferation characteristics and integrin expression shows marked differences in these parameters, which may correlate with enhanced invasiveness[23] (Fig. 1c and Supplementary Fig. 4). Because cell–cell adhesion within tissue will regulate the perimeter stress, we designed straight line and torus geometries where curvature and perimeter/area can be varied. After five days of culture we see that both perimeter curvature

[1]Department of Materials Science and Engineering, University of Illinois at Urbana-Champaign, Urbana, Illinois 61801, USA. [2]Department of Pathobiology, University of Illinois at Urbana-Champaign, Urbana, Illinois 61801, USA. [3]Department of Veterinary Clinical Medicine, University of Illinois at Urbana-Champaign, Urbana, Illinois 61801, USA. *e-mail: kakilian@illinois.edu

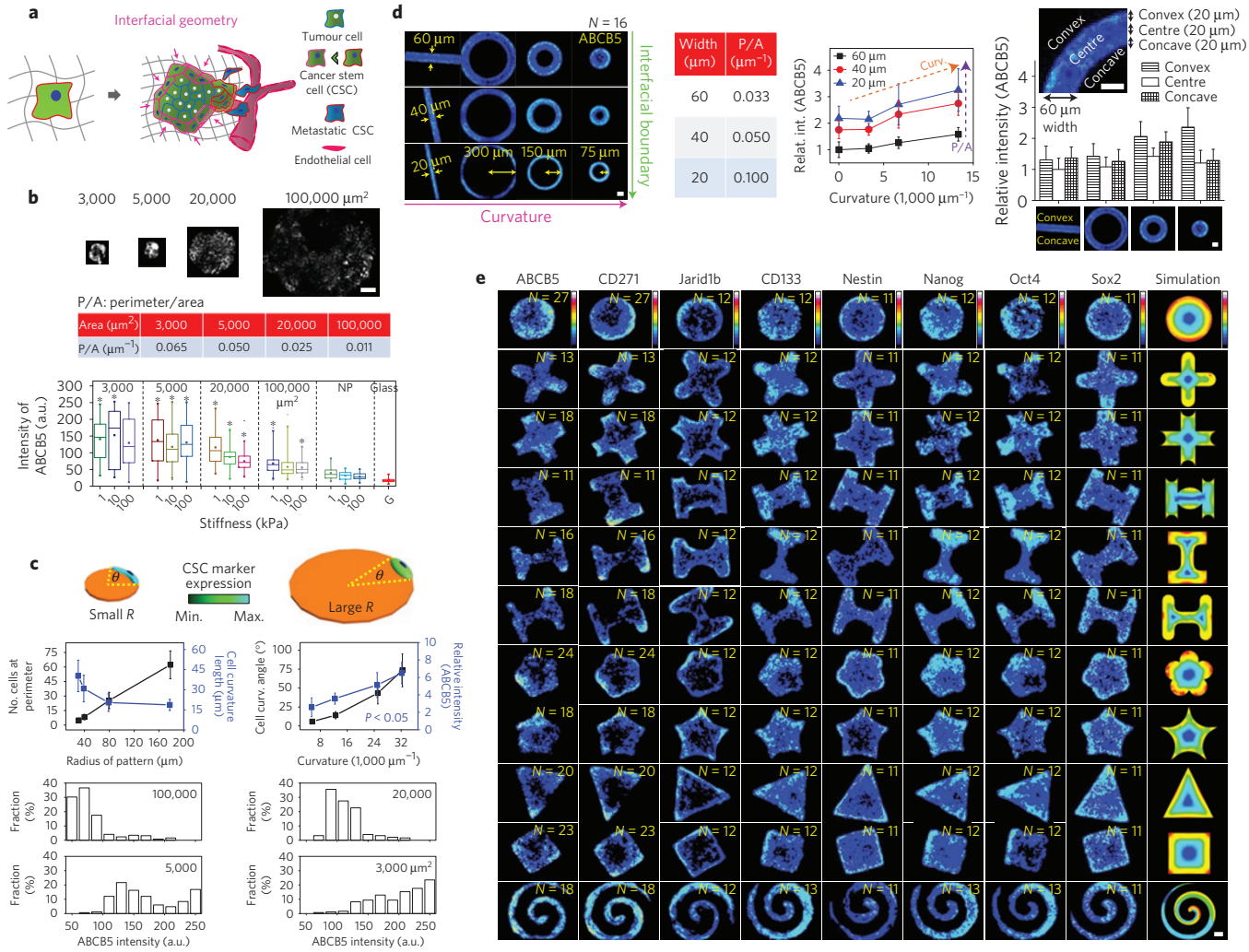

Figure 1 | Interfacial geometry at perimeter features directs expression of CSC markers. a, Schematic depicting how extracellular matrix properties may guide tumorigenicity. **b**, Increasing micropattern size shows optimal curvature that guides expression of CSC markers in B16F0 cells ($N=3$, $^*P<0.05$, Fisher's exact test compared to glass); boxes represent 25th to 75th percentile and whiskers represent minimum–maximum. Horizontal lines and points within boxes represent the median and mean respectively for three replicates. **c**, Curvature influences expression of CSC molecular markers. Intensity of ABCB5 shown as fold change over the non-patterned (NP) condition ($N=3$). (*P*-value from ANOVA analysis). *R*, pattern radius. **d**, Shapes controlling line width, curvature and perimeter to area ratio to explore the relationship of interfacial geometry and expression of CSC markers ($N=3$). **e**, Immunofluorescence heatmaps of B16F0 cells cultured in a panel of shapes with variable perimeter geometric features showing semiquantitative localization characteristics for CSC surface markers (ABCB5, CD271, CD133), slow-cycling related demethylase enzyme (JARID1B), intermediate filaments (Nestin) and transcription factors (Nanog, Oct4, Sox2). Far right column shows finite element models of perimeter stress in cellular sheets. Colour bar indicates minimum (bottom) to maximum (top) intensity. Scale bars, 50 μm. Error bars represent s.d.

and perimeter–area ratio (a measure proportional to interfacial energy[24]) exert an influence on the expression of perimeter CSC markers. In all cases, convex curvature at the exterior of the torus shows higher expression of CSC markers compared to interior concave regions (Fig. 1d and Supplementary Fig. 5).

We designed a range of patterns comprising edges, concave and convex regions, corners of different angles and various radii of curvature, to investigate how combinations of interfacial cues at the perimeter of a population of tumour cells guide cellular organization and the expression of CSC markers (Supplementary Fig. 6). Across all shapes we see higher expression of CSC markers near the periphery, with higher expression localized to convex features and corners. We note a degree of anisotropy in some of our heatmaps, which may be due to uneven initial seeding or patterning artefacts. To further verify our trends in spatial immunofluorescence, we performed segmentation analysis of CSC markers across our pattern features (Supplementary Figs 7 and 8). To evaluate whether these cells show other characteristics of stem cells, we stained for molecular markers of pluripotency and tumorigenic phenotypes, including intermediate filaments (Nestin), chromatin modifying enzymes (Jarid1b) and transcription factors (Oct4, Sox2, Nanog). Strikingly, these markers co-localized with the CSC markers. We used finite element analysis to construct a simple model of the relative mechanical stress distribution of a contractile patterned monolayer, and found good correspondence between 'hotspots' of high CSC marker expression and regions of enhanced mechanical stress within multicellular sheets (Fig. 1e and Supplementary Figs 9 and 10). Because perimeter features in cell islands, both convex and concave, give rise to cells with higher expression of CSC markers compared to cells in the interior, we designed a spiral geometry with a high interfacial boundary (perimeter/area) that exhibits an increasing radius of curvature encompassing the range depicted

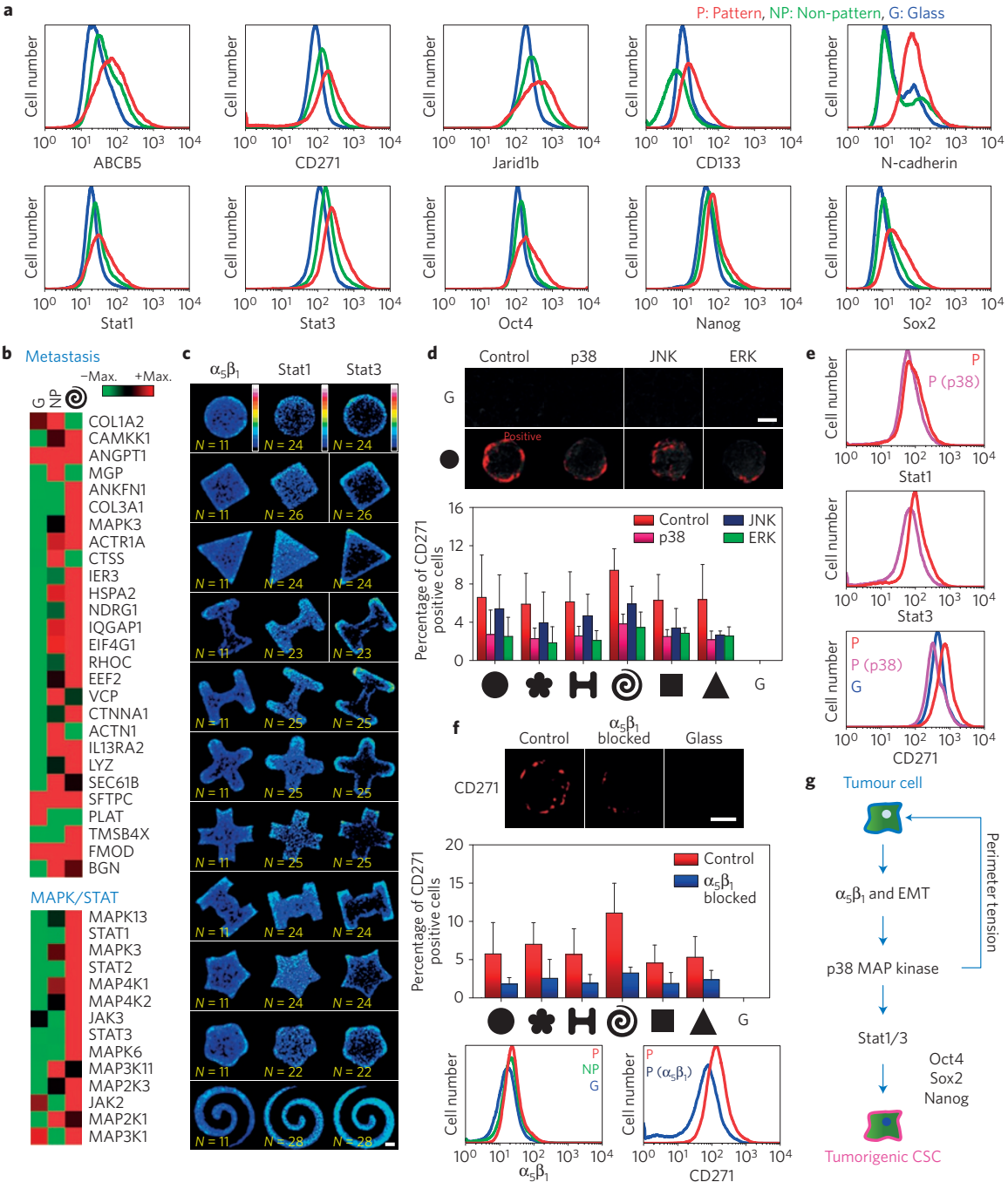

Figure 2 | Geometric cues activate CSCs at the perimeter through integrin α5β1, mitogen-activated protein kinase (MAPK) signalling and regulation of signal transducer and activator of transcription (STAT) pathways. a, Flow cytometry characterization of markers associated with epithelial to mesenchymal transition, CSC state and pluripotency in B16F0 cells. **b**, Gene expression analysis of transcripts associated with metastatic potential and MAPK/STAT signalling for cells cultured on glass (G), non-patterned hydrogel (NP) and spiral-patterned hydrogel. **c**, Immunofluorescence heatmaps of $\alpha_5\beta_1$, Stat1 and Stat3 for B16F0 cells patterned on our panel of geometries. Colour bar indicates minimum (bottom) to maximum (top) intensity. **d**, CD271 expression in B16F0 cells following treatment with pharmacological inhibitors of MAPK pathways ($N=3$). **e**, Flow cytometry characterization of CD271, Stat1 and Stat3 positive cells with p38 inhibition. **f**, CD271 expression in B16F0 cells on treatment with blocking antibodies against integrin $\alpha_5\beta_1$ ($N=3$). **g**, Proposed pathway for interfacial geometry guiding tumorigenicity. Error bars represent s.d. Bold shapes depict the cell culture geometries. Scale bar, 50 μm.

in Fig. 1d. Cells cultured in the spiral shape demonstrate high expression of markers associated with a CSC state (Fig. 1e). We selected cells cultured on this shape for flow cytometry analysis using both B16F0 and B16F10 melanoma cells cultured for five days. Similar to the immunofluorescence results, cells cultured in the spiral patterns show higher levels of stem cell and tumorigenicity markers compared to those cultured on non-patterned surfaces and those on glass (Fig. 2a and Supplementary Fig. 11).

To gain insight into how interfacial geometry may exert an influence on the CSC state, we performed a full genome expression analysis. B16F0 and B16F10 cells were grown on spiral-patterned PA gels, non-patterned PA gels, and glass substrates for five

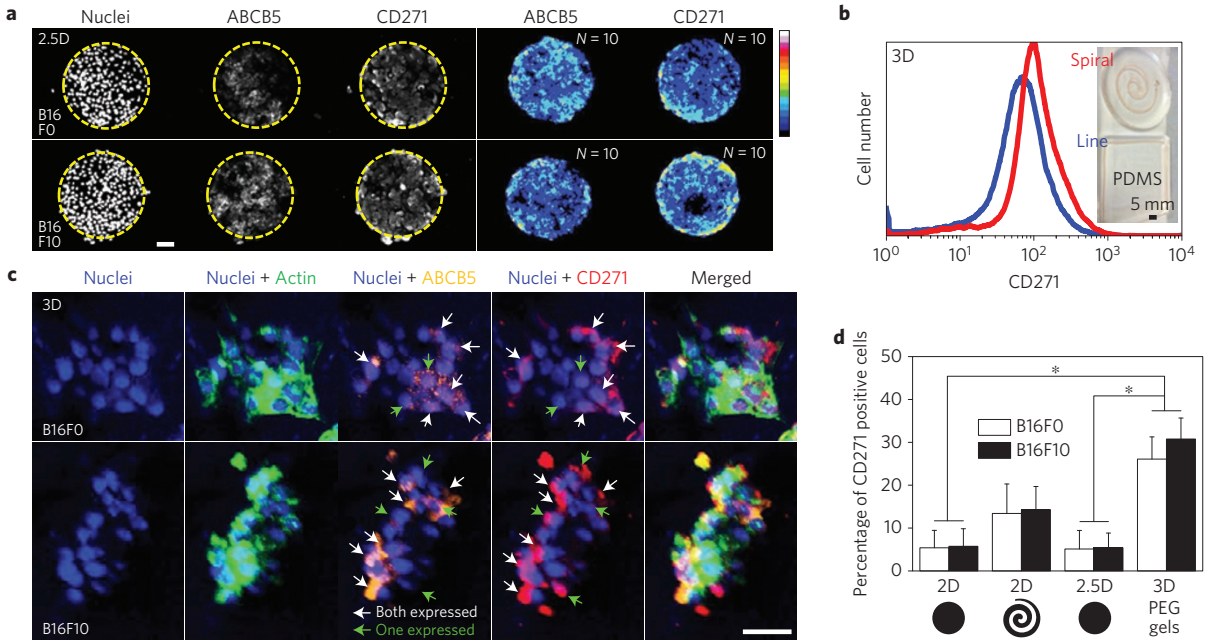

Figure 3 | Cells encapsulated in model 3D microenvironments demonstrate interfacial regulation of the CSC phenotype. a, Representative immunofluorescence microscopy images and immunofluorescence heatmaps of B16F0 and B16F10 cells captured within polyacrylamide (PA) pseudo-3D (2.5D) microwells with large areas (50,000 μm^2). Colour bar indicates minimum (bottom) to maximum (top) intensity. **b**, Flow cytometry characterization of CSC markers expressed at the perimeter within a PDMS microfluidic device with 3D spiral and linear channels. **c**, Encapsulated B16F0 and B16F10 cells in matrix metalloprotease (MMP)-degradable PEG gels showing increased localization of CSC markers at the perimeter of aggregates. Approximately 30% of cells expressing either ABCB5 or CD271 did not express both CSC markers at the same time. **d**, The fraction of B16F0 cells positive for CD271 in different dimensional synthetic model systems. The glass control was used to generate thresholds of the marker intensity for different substrates ($N=3$). Scale bar, 50 μm. ($^*P < 0.05$, Fisher's exact test). Error bars represent s.d. Bold shapes depict the cell culture geometries.

days, followed by RNA isolation and gene expression analysis. Hierarchical clustering demonstrates segregation of B16F0 and B16F10 cells, as well as those cultured on patterned and non-patterned gels compared to glass. A panel of metastasis-related transcripts, mitogen-activated protein kinase cascades (MAPK), and signal transducers and activators of transcription (STAT) show higher levels of expression in both cell lines (B16F0 and B16F10) cultured on the patterns relative to cells cultured on non-patterned gels and glass substrates (Fig. 2b and Supplementary Fig. 12). Immunostaining for integrin $\alpha_5\beta_1$, Stat1 and Stat3 in patterned B16F0 and B16F10 cells shows elevated expression at the perimeter features, similar to the signature found with CSC markers and stem cell transcription factors (Fig. 2c and Supplementary Fig. 13). Cells cultured on spiral shapes exhibit elevated expression of genes involved in the MAP kinase pathways linked to mechanotransduction, particularly p38 kinases and extracellular related kinases (ERK). To determine the extent to which MAPK signalling transduces signals within cells along the perimeter curvature, we supplemented our patterned culture with pharmacological inhibitors of MAPK pathways. Addition of a p38 inhibitor and an ERK 1/2 inhibitor led to a decrease in the expression of CSC markers at the perimeter, whereas addition of a JNK inhibitor resulted in more subtle, shape-dependent changes (Fig. 2d and Supplementary Fig. 14a). Because STAT transcriptional activity can be elevated through p38 MAPK signalling cascades[25] and has been shown to play a role in melanoma progression[26], we also explored the ability of p38 inhibition to modulate STAT activity. Supplementing the patterned cultures with p38 inhibitor attenuated Stat1 and Stat3 perimeter localization as determined by both immunofluorescence and flow cytometry (Fig. 2e and Supplementary Fig. 14b). In addition, introduction of blocking antibodies against $\alpha_5\beta_1$ during culture leads to a partial reduction in the expression of melanoma CSC markers (Fig. 2f and Supplementary Fig. 7c), suggesting integrin $\alpha_5\beta_1$ plays a role in CSC adhesion. Taken together, we propose that interfacial geometry will modulate cell shape, and enhance $\alpha_5\beta_1$ adhesion, MAPK signalling and STAT activity to promote initiation of self-renewal stem cell networks (Fig. 2g).

Recently we demonstrated how switching the biophysical microenvironment could rewire cell state using mesenchymal stem cells as a model system[27]. Using this platform we explored whether switching the microenvironments between patterned and glass substrates could rewire the tumorigenic CSC state. Cells were cultured on both types of substrate for five days, followed by transfer of spiral-patterned cells to glass and vice versa. Transfer of B16 cells from glass to patterned substrates led to increased expression of CSC markers, whereas cells transferred from patterned to glass substrates maintained some elevation of ABCB5 and CD271 after five days, suggesting the CSC state remains initially stable after removal from the patterns (Supplementary Fig. 15).

In our model 2D tumour microenvironments, interfacial geometry will promote signalling that establishes a tumorigenic CSC state. During tumour growth *in vivo*, stiffening matrices will similarly present regions of high interfacial tension at the perimeter of the growing tumour[1]. To ask whether interfaces in higher-dimensional materials—that more closely recapitulate an *in vivo* environment—can similarly activate a tumorigenic state, we used a templating approach to fabricate pseudo-3D microwells of PA gels (Fig. 3a), a 3D microfluidics polydimethylsiloxane (PDMS) device with varying geometry (Fig. 3b), or encapsulating groups of cells in 3D poly(ethylene glycol) (PEG) gels, all either coated or conjugated with fibronectin (Fig. 3c). After five days in culture, cells at the perimeter express higher levels of CSC markers in all of these experimental architectures. The consistent enhancement of CSC markers at the perimeter of our 2D and 3D tumour models gives credence to the idea that interfacial geometry may prove a general

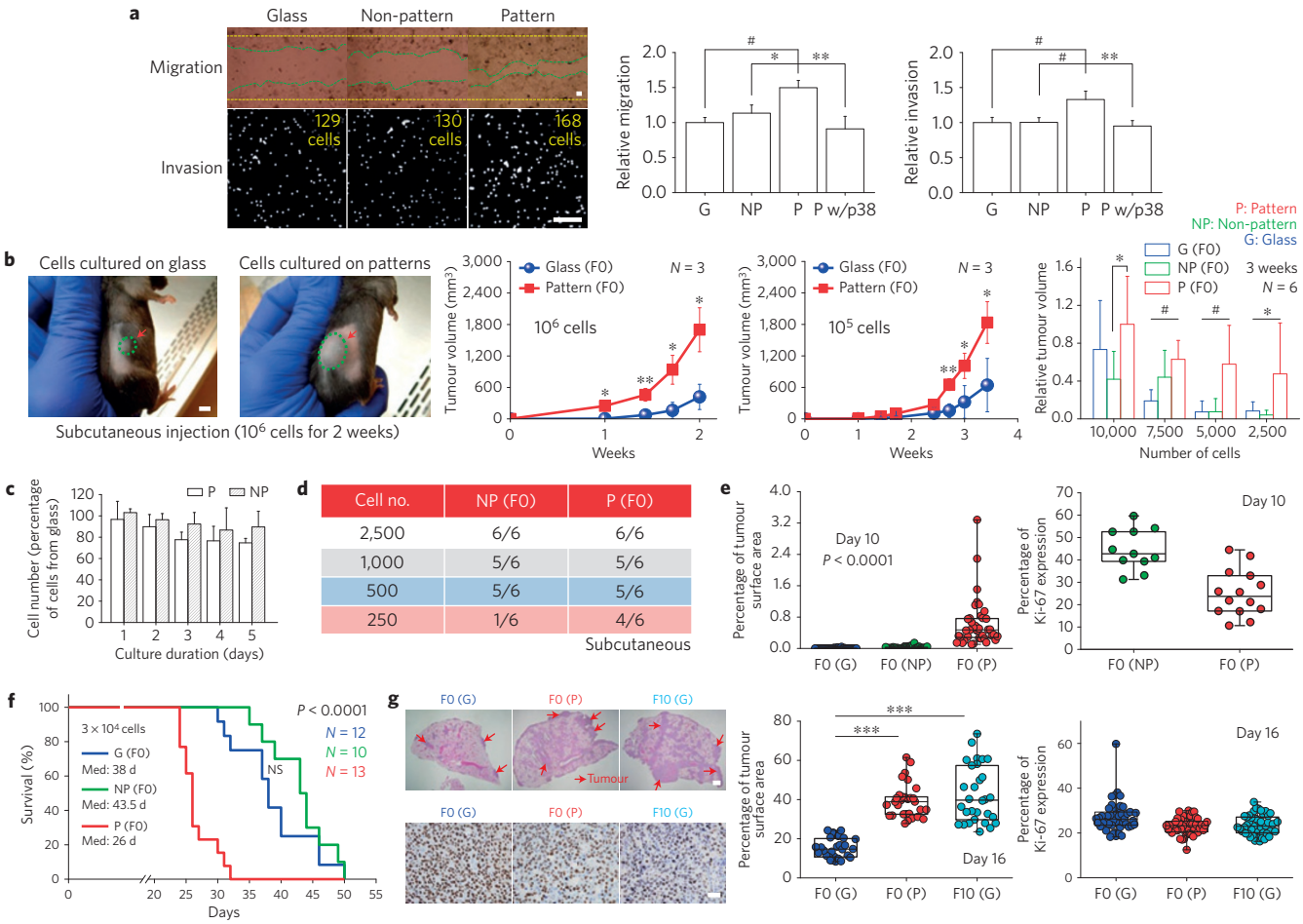

Figure 4 | Activated cells show higher tumorigenicity and metastatic potency *in vivo*. **a**, Wound healing and Boyden chamber invasion assays for B16F0 (F0) cells cultured on glass, non-patterned gels, spiral-patterned gels, and on spiral-patterned gels with p38 inhibition. Scale bar, 100 μm ($N=3$, $^{*}P<0.05$, $^{\#}P<0.01$, $^{**}P<0.005$ based on ANOVA with Tukey HSD post hoc testing). **b**, Tumour growth characteristics of subcutaneous implanted cells in C57BL/6 mice. Scale bar, 5 mm. **c**, Proliferation characteristics of patterned (P) and non-patterned (NP) cells relative to those cultured on glass ($N=3$, $^{*}P<0.05$, $^{\#}P<0.01$, $^{**}P<0.005$ based on ANOVA with Tukey HSD post hoc testing). **d**, Tumorigenicity results (number of mice that develop tumours) after limited dilutions of B16F0 cells from non-patterned gels or spiral-patterned gels after 60 days implantation in C57BL/6 mice. **e**, Tumour surface area (at day 10) and proliferation assessment through Ki67 staining (at day 10) of excised lung tissue after experimental metastasis. (*P*-value from ANOVA analysis, *N* is the number of lung sections used). **f**, Kaplan–Meier analysis of C57BL/6 mice after experimental metastasis. (*P*-value from ANOVA analysis; Med., median survival time (days)). **g**, Histopathology of lung sections after pulmonary metastasis and immunolabelling of excised lung tissue stained for Ki67 markers after tail vein injection of B16F0 cells cultured on glass or in the spiral geometry, compared to the highly metastatic B16F10 cells (F10; positive, brown; negative, blue). (*N* is the number of lung sections used, $^{***}P<0.0005$ based on ANOVA with Tukey HSD post hoc testing). Error bars represent s.d.—except for **e** and **g**, where boxes represent 25th to 75th percentile and whiskers represent minimum–maximum. Scale bar, 1 mm for histopathology images and 50 μm for Ki67 staining.

driver in coordinating cell state during oncogenesis en route to metastasis (Fig. 3d).

To explore the metastatic potential and tumorigenicity of our engineered cells, we performed a number of *in vitro* and *in vivo* analyses. Wound healing and Boyden chamber invasion assays demonstrate enhanced migration and invasion characteristics for cells initially cultured on spiral patterns, and p38 inhibition abrogates these trends (Fig. 4a and Supplementary Fig. 16). For an *in vivo* test of tumorigenicity, B16F0 cells were cultured for five days on spiral-patterned gels, non-patterned gels or glass substrates, followed by subcutaneous injection into 6–8-week-old C57BL/6 mice; primary tumour establishment and growth were monitored every three days with callipers. Primary tumour growth was significantly enhanced for the B16F0 cells cultured on patterned gels compared to cells cultured on non-patterned gels or glass (Fig. 4b). To probe the differences in growth rates for the B16 cells, we cultured cells on spiral-patterned gels, non-patterned gels or glass substrates for five days, followed by trypsinization and re-seeding on glass. Division rates were similar for both conditions (Fig. 4c), suggesting enhanced tumour growth *in vivo* for the engineered cells is due either to enhanced proliferation *in vivo* or on account of better survival characteristics. We performed a limited dilution study to evaluate tumorigenicity, where mice were inoculated with suspensions of 2,500, 1,000, 500 and 250 cells from our spiral-patterned gel and non-patterned gel condition. After two months we see that 4 of the 6 mice at the lowest dilution have developed tumours from spiral-patterned cells, compared to 1 of 6 in mice injected with cells from non-patterned gels (Fig. 4d). This result suggests cells from our patterned hydrogels exhibit enhanced tumorigenicity. With the observed difference for primary tumour growth, we sought to confirm if engineered cells would likewise possess enhanced metastatic potency. We induced experimental metastasis by tail vein injection in C57BL/6 mice of three conditions: B16F0 cells cultured on glass, B16F0

cells cultured on non-patterned gels, and B16F0 cells cultured on spiral-patterned gels. After 5 and 10 days, a cohort of mice were euthanized and histopathology performed on the lungs, with metastatic burden calculated as a normalized percentage tumour surface area. B16F0 cells cultured on spiral patterns show higher metastatic burden compared with those cultured on glass or non-patterned gels (Fig. 4e and Supplementary Fig. 17a and b). Correspondingly, Kaplan–Meier analysis demonstrates that mice inoculated with 3.0×10^4 F0 cells cultured on non-patterned gels or glass survived the longest, whereas cells grown on spiral geometries demonstrated truncated survival times (Fig. 4f). We measured early stage (Day 10) B16 F0 proliferation after metastasis (2.5×10^5 cells) and found similar proliferation, albeit slightly higher for cells inoculated from the non-patterned gel condition (Fig. 4e and Supplementary Fig. 17c). Considering the significantly higher tumour burden observed in lungs from mice inoculated with patterned cells, this suggests metastatic burden does not arise from increased proliferation, but rather from improved survival characteristics consistent with increased tumorigenicity. We also performed experimental metastasis to compare B16F0 cells with the highly metastatic B16F10 cells cultured on glass. Kaplan–Meier analysis shows that mice inoculated with B16F0 cells survived the longest, with comparable truncated survival times for B16F10 cells and B16F0 cells grown on spiral patterns (Fig. 4g and Supplementary Fig. 17d). We have shown how interfacial geometry can activate a stem-cell state *in vitro* (Supplementary Fig. 8); however, our *in vivo* experiments with the spiral-patterned gels remain inconclusive as to whether curvature or the sole presence of the interface regulates cancer-cell state. Future work exploring cells patterned in other shapes that isolate positive and negative curvature may prove useful in discerning how subtle changes in perimeter geometry may guide tumorigenicity. Furthermore, it remains to be demonstrated whether curvature at the interface in a growing tumour will prime a highly metastatic CSC state.

To ascertain whether the influence of geometry may prove to serve as a universal tumorigenicity guidance cue, we immunostained several other cancer types for the generation of heatmaps. Similar to murine B16F0 and B16F10 melanoma cells, several human cancers; human HeLa (cervical), A549 (lung), and PC3 (prostate) cell lines, all showed similar trends in CSC marker expression on 10 kPa gels (Supplementary Fig. 18). These findings suggest that interfacial geometry may prove to be a general biophysical phenomena underlying cancer cell progression within a microenvironment.

Our results demonstrate how the interfacial constraints imposed by perimeter geometric features in a population of tumour cells can guide cancer cells towards a stem-cell-like state. *In vivo*, the balance between intercellular adhesion and cortical tension act together to specify tissue surface tension[24], which regulates the local behaviour of groups of cells[28,29]. Similarly, the state of a tumour cell in a multicellular aggregate may depend on the interplay between force balance, cellular tension, intercellular adhesion and relative position with respect to other cells[30]. In line with this hypothesis, we find that perimeter curvature can coordinate the spatial arrangement of cells by modifying interfacial energy, cortical tension and intercellular adhesion. We show that this coordination can foster a unique microenvironment where integrin-mediated adhesion and mechanotransduction activate a CSC phenotype. Our findings are in contrast to previous studies where 'stemness' is promoted in regions of low mechanical tension[9,31], which suggests interfacial geometry may play a unique role in cancer through activation of a stem-like cell with a role in metastasis. This finding may help guide clinical analysis of the tumour microenvironment during biopsy or resection, and may lead to advances in the design, development and translation of patient-specific models of oncogenesis for personalized therapeutic development.

Methods

Methods and any associated references are available in the online version of the paper.

Received 4 June 2015; accepted 25 February 2016; published online 4 April 2016

References

1. Lu, P., Weaver, V. M. & Werb, Z. The extracellular matrix: a dynamic niche in cancer progression. *J. Cell Biol.* **196,** 395–406 (2012).
2. Visvader, J. E. & Lindeman, G. J. Cancer stem cells in solid tumours: accumulating evidence and unresolved questions. *Nature Rev. Cancer* **8,** 755–768 (2008).
3. Hanahan, D. & Weinberg, R. A. Hallmarks of cancer: the next generation. *Cell* **144,** 646–674 (2011).
4. Mehlen, P. & Puisieux, A. Metastasis: a question of life or death. *Nature Rev. Cancer* **6,** 449–458 (2006).
5. Dean, M., Fojo, T. & Bates, S. Tumour stem cells and drug resistance. *Nature Rev. Cancer* **5,** 275–284 (2005).
6. Magee, J. A., Piskounova, E. & Morrison, S. J. Cancer stem cells: impact, heterogeneity, and uncertainty. *Cancer Cell* **21,** 283–296 (2012).
7. Roesch, A. *et al*. A temporarily distinct subpopulation of slow-cycling melanoma cells is required for continuous tumor growth. *Cell* **141,** 583–594 (2010).
8. Liu, J. *et al*. Soft fibrin gels promote selection and growth of tumorigenic cells. *Nature Mater.* **11,** 734–741 (2012).
9. Tan, Y. *et al*. Matrix softness regulates plasticity of tumour-repopulating cells via H3K9 demethylation and Sox2 expression. *Nature Commun.* **5,** 4619 (2014).
10. Kumar, S. & Weaver, V. M. Mechanics, malignancy, and metastasis: the force journey of a tumor cell. *Cancer Metastasis Rev.* **28,** 113–127 (2009).
11. Discher, D. E., Janmey, P. & Wang, Y. L. Tissue cells feel and respond to the stiffness of their substrate. *Science* **310,** 1139–1143 (2005).
12. Swift, J. *et al*. Nuclear Lamin-A scales with tissue stiffness and enhances matrix-directed differentiation. *Science* **341,** 1240104 (2013).
13. Ingber, D. E. Mechanical control of tissue growth: function follows form. *Proc. Natl Acad. Sci. USA* **102,** 11571–11572 (2005).
14. Nelson, C. M. *et al*. Emergent patterns of growth controlled by multicellular form and mechanics. *Proc. Natl Acad. Sci. USA* **102,** 11594–11599 (2005).
15. Friedl, P. & Gilmour, D. Collective cell migration in morphogenesis, regeneration and cancer. *Nature Rev. Mol. Cell Biol.* **10,** 445–457 (2009).
16. Nelson, C. M., Vanduijn, M. M., Inman, J. L., Fletcher, D. A. & Bissell, M. J. Tissue geometry determines sites of mammary branching morphogenesis in organotypic cultures. *Science* **314,** 298–300 (2006).
17. Murphy, W. L., Mcdevitt, T. C. & Engler, A. J. Materials as stem cell regulators. *Nature Mater.* **13,** 547–557 (2014).
18. Gomez, E. W., Chen, Q. K., Gjorevski, N. & Nelson, C. M. Tissue geometry patterns epithelial–mesenchymal transition via intercellular mechanotransduction. *J. Cell. Biochem.* **110,** 44–51 (2010).
19. Boghaert, E. *et al*. Host epithelial geometry regulates breast cancer cell invasiveness. *Proc. Natl Acad. Sci. USA* **109,** 19632–19637 (2012).
20. Medema, J. P. Cancer stem cells: the challenges ahead. *Nature Cell Biol.* **15,** 338–344 (2013).
21. Boiko, A. D. *et al*. Human melanoma-initiating cells express neural crest nerve growth factor receptor CD271. *Nature* **466,** 133–137 (2010).
22. Frank, N. Y. ABCB5-mediated doxorubicin transport and chemoresistance in human malignant melanoma. *Cancer Res.* **65,** 4320–4333 (2005).
23. Sil, H., Sen, T. & Chatterjee, A. Fibronectin-integrin ($\alpha_5\beta_1$) modulates migration and invasion of murine melanoma cell line B16F10 by involving MMP-9. *Oncol. Res.* **19,** 335–348 (2011).
24. Manning, M. L., Foty, R. A., Steinberg, M. S. & Schoetz, E. M. Coaction of intercellular adhesion and cortical tension specifies tissue surface tension. *Proc. Natl Acad. Sci. USA* **107,** 12517–12522 (2010).
25. Roux, P. P. & Blenis, J. ERK and p38 MAPK-activated protein kinases: a family of protein kinases with diverse biological functions. *Microbiol. Mol. Biol. Rev.* **68,** 320–344 (2004).
26. Nicholas, C. & Lesinski, G. B. in *The Jak-STAT signal transduction pathway in melanoma*, 283–306 (Breakthroughs in Melanoma Research, 2011).
27. Lee, J., Abdeen, A. A. & Kilian, K. A. Rewiring mesenchymal stem cell lineage specification by switching the biophysical microenvironment. *Sci. Rep.* **4,** 5188 (2014).
28. Lecuit, T. & Lenne, P. F. Cell surface mechanics and the control of cell shape, tissue patterns and morphogenesis. *Nature Rev. Mol. Cell Biol.* **8,** 633–644 (2007).

29. Kollmannsberger, P., Bidan, C. M., Dunlop, J. W. C. & Fratzl, P. The physics of tissue patterning and extracellular matrix organisation: how cells join forces. *Soft Matter* **7,** 9549–9560 (2011).
30. Hegerfeldt, Y., Tusch, M., Bröcker, E. B. & Friedl, P. Collective cell movement in primary melanoma explants. *Cancer Res.* **62,** 2125–2130 (2002).
31. Lee, J., Abdeen, A. A., Kim, A. & Kilian, K. A. The influence of biophysical parameters on maintaining the mesenchymal stem cell phenotype. *ACS Biomater. Sci. Eng.* **1,** 218–226 (2015).

Acknowledgements

This research was supported with funding from the American Cancer Society Illinois Division Grant # 281225 and the National Science Foundation Grant # 1454616 CAR. Graduate student (K.L.W.) support was provided by Morris Animal Foundation. We thank the Beckman Institute ITG facilities, Institute of Genomic Biology Imaging facilities, Micro and Nanotechnology Laboratory facilities, and the Roy J. Carver Biotechnology Center.

Author contributions

J.L. and K.A.K. conceived the ideas and designed the experiments. J.L., A.A.A., K.L.W. and T.M.F. conducted the experiments. J.L., A.A.A., K.L.W., T.M.F. and K.A.K. analysed the data. J.L., A.A.A., T.M.F. and K.A.K. interpreted the data and wrote the manuscript.

Additional information

Supplementary information is available in the online version of the paper. Reprints and permissions information is available online at www.nature.com/reprints. Correspondence and requests for materials should be addressed to K.A.K.

Competing financial interests

The authors declare no competing financial interests.

Methods

2D and 3D surface preparation. For 2D polyacrylamide (PA) hydrogels, we used the previously reported protocol[32]. Briefly, PA gels with desired stiffness (1, 10 and 100 kPa) were fabricated on a glass coverslip (18 mm, Fisher Scientific) by mixing varying amounts of acrylamide and bis-acrylamide (Sigma). 0.1% ammonium persulfate (APS, Sigma) and 0.1% tetramethylethylenediamine (TEMED, Sigma) were added to initiate the reaction. Activated coverslips were functionalized with 3-aminopropyltriethoxysilane for 3 min and glutaraldehyde for 30 min (Sigma) and then 20 µl of gel solution was sandwiched between the activated coverslips and a hydrophobically treated glass slide. The gel-coated coverslips were gently detached after an appropriate polymerization time for each stiffness condition. The gel surfaces were treated with hydrazine hydrate (55%, 2 h) to modify the surface chemistry and then rinsed with 5% glacial acetic acid (1 h) followed by distilled water (1 h; ref. 33). Patterned or non-patterned polydimethylsiloxane (PDMS, Polysciences) stamps of desired shapes were produced by using photolithography. To create patterned stamps, PDMS was polymerized on a patterned master of photoresist (SU-8, MicroChem) created using ultraviolet photolithography through a laser printed mask. Free aldehydes were generated on fibronectin (25 µg ml^{-1}, Sigma) in PBS by adding sodium periodate (~3.5 mg ml^{-1}, Sigma) for at least 45 min. The protein solution was pooled onto patterned or non-patterned (flat) stamps for 30 min and dried with air. The protein residues on stamps were transferred to the gel surface through covalent conjugation of free aldehyde groups in proteins to reactive hydrazide groups on the gels.

For pseudo-3D microwells, an SU-8 photolithography master exhibiting the inverse features used in fabricating the PDMS stamps was used as a template to cast PA gels with microwells on the surface. The gels were chemically modified with hydrazine hydrate and the oxidized protein solution was applied. To render the external surface non-adhesive, the top layer of protein-conjugated gels was sheared off by applying an adhesive strip to the surface. In all of our experiments we ensured cells formed only a single monolayer, to ensure uniform antibody staining.

For 3D poly(ethylene glycol) (PEG) gels, 10,000 MW PEG (Sigma) was modified to poly(ethylene glycol) diacrylate (PEGDA), as previously reported, by the addition of acryloyl chloride[34]. Fibronectin was acrylated by the addition of NHS-Acrylate (Sigma) under basic pH for 4 h. Matrix metalloprotease (MMP) cleavable peptides were synthesized using solid phase peptide synthesis and reacted with PEGDA via Michael addition of terminal cysteine residues. 3-(trimethoxysilyl)propyl methacrylate 2% solution in ethanol with 0.3% glacial acetic acid was applied to coverslips for 10 min for activation, followed by baking at 95C for 1 h[35]. To encapsulate cells in the degradable hydrogels, 30% (w/v) PEGDA–MMP was mixed with ultraviolet-initiator (0.05% Irgacure 2959, Sigma) and cells were centrifuged and re-suspended in this mixture. This solution was sandwiched between the activated coverslip and a hydrophobic coverslip. Ultraviolet light (5 mW cm^{-2}) was applied for 10 min and the encapsulated cells were detached and placed in cell culture media. For 3D microfluidics PDMS devices, flexible rubber-coated wire (200 mm long, 2 mm diameter) was employed to design microfluidic devices with different shapes. The designed wire (line or spiral) was placed on the first layer of PDMS (flat) and the second layer of PDMS was fabricated with the wire inside. After the wire was removed from the PDMS, 0.2 mg ml^{-1} sulfosuccinimidyl 6 (4′-azido-2′-nitrophenyl-amino) hexanoate (Sulfo-SANPAH; Pierce), a heterobifunctional protein crosslinker, was used to covalently bind proteins to the PDMS channel inside; exposure of the PDMS in a solution of Sulfo-SANPAH with an ultraviolet light source at 365 or 320 nm covalently linked the sulfo-SANPAH to the PDMS (1 h). Sulfo-SANPAH solution was removed from the PDMS channel and the device was washed by gently adding and aspirating PBS until the PDMS channel was transparent again. Fibronectin (25 µg ml^{-1}) was conjugated on the surface-modified PDMS inside the channel for 24 h.

Cell source and culture. The cancer cell lines B16F0 and B16F10 (murine melanoma), and PC3 (human prostate) were obtained from American Type Culture Collection (ATCC) and cultured according to the recommended protocols. HeLa (human cervical, ATCC) cells were a gift from Andrew M. Smith's laboratory; A549 (human lung, ATCC) cells were a kind gift from Jianjun Cheng's laboratory. For cell culture, media was changed every three days and cells were passaged at nearly 90% confluence using 0.25% trypsin (Gibco). B16 cells were tested for mycoplasma contamination at Charles River Laboratories for cell line testing prior to *in vivo* inoculation.

Immunofluorescence. Cells were fixed with 4% paraformaldehyde (Sigma) for 20 min and permeabilized in 0.1% Triton X-100 (Fisher) in PBS for 30 min. 1% Bovine serum albumin (BSA) was employed to block the cells for 15 min and primary antibody labelling was performed in 1% BSA in PBS for 2 h at room temperature, followed by rinsing with PBS two times. Secondary antibody labelling was performed in 2% goat serum, 1% BSA in PBS for 20 min in a humid chamber (5% CO_2 and 37 °C). Immunofluorescence microscopy was conducted using a Zeiss Axiovert 200 M inverted research-grade microscope (Carl Zeiss) or an LSM 700 (Carl Zeiss), which is a four laser, point scanning confocal with a single pinhole. Antibodies used for immunostaining, flow cytometry, and immunohistochemistry are listed in Supplementary Table 1.

Inhibition assays. MAP kinase inhibitions (FR180204 (ERK1/2), SP600125 (JNK), and SB202190 (p38)) (Calbiochem) were performed by adding media supplemented with these inhibitors at 6 µM concentration after cell seeding and with each media change. Integrin-blocking antibodies ($\alpha_5\beta_1$) were added to cells in media before seeding at 1 µg ml^{-1}.

Wound healing assay. B16F0 and B16F10 cells were cultured for five days on spiral patterns (with or without p38 inhibitors), non-patterned gels, or glass substrates (12 identical substrates). Cells were trypsinized and re-plated on glass substrates (10^6 cells per glass) and then cultured under permissive condition to about 90% confluence. A pipet tip was employed to create a linear scratch in the confluent monolayer. Cells were allowed to migrate and close the wound for 12 h, and were observed under phase contrast microscopy. The scratch width per field of view, between the time points 0 and 12 h following wound closure, was determined using imageJ[36], and the average percentage of wound closure, indicated by the shifted width after 12 h, was assessed.

Boyden chamber assay. Invasion of B16F0 and B16F10 cells was examined using 24-well Boyden chambers (Corning) with inserts (8 µm pores) and precoated basement membrane extract (Matrigel, growth factor reduced) (BD Biosciences). Cells were cultured for five days on spiral patterns (with or without p38 inhibitors), non-patterned gels or glass substrates (12 identical substrates) and then placed on the inserts in the upper chambers (of each well) and cultured for 12 h. Cells on the upper surface of the membrane filter were removed. Cells that crossed the inserts to the lower surface were fixed with 4% paraformaldehyde and then stained with 4′,6-diamidino-2-phenylindole (DAPI). Cells per field of view were imaged under a ×10 fluorescence microscope and counted.

Cell labelling and flow cytometry. B16F0 and B16F10 cells cultured for five days on spiral patterns or glass substrates (12 identical substrates) were trypsinized and broken down into a single cell suspension. Cells were fixed in 4% paraformaldehyde for 20 min and permeabilized in 0.1% Triton X-100 in PBS for 15 min. Cells were blocked in 1% BSA for 1 h. Cells were stained with primary antibodies in 1% BSA in PBS for 2 h at room temperature. Next, secondary antibodies in 2% goat serum, 1% BSA in PBS were applied for 20 min in a humid chamber (5% CO_2 and 37 °C). Before every step, cells were washed three times with PBS. Flow cytometry analysis was performed with a BD LSR Fortessa Flow Cytometry Analyzer. Cells stained without primary antibodies were used as negative controls to set the baseline.

Cell proliferation assay *in vitro*. BrdU staining was conducted as reported previously[37]. Briefly, BrdU labelling reagent (Invitrogen) was added (1:100 v/v) before 24 h of fixing; the reagent was added after seeding, day 2, or day 4 for fixing at days 1, 3, or 5, respectively. Cells were fixed in 70% ethanol for 30 min and then denatured with 2 M HCl for 30 min. Cells were permeabilized with 0.1% Triton X-100 in PBS for 30 min, blocked with 1% BSA in PBS for 15 min, and then incubated with mouse anti-BrdU primary antibody (3 h at room temperature) followed by Alexa Fluor 647-conjugated antimouse IgG antibody (20 min in a humid chamber). Cell nuclei were stained with DAPI. For the division rate assay, B16F0 and B16F10 cells cultured for five days on spiral patterns or glass substrates (six identical substrates) were trypsinized and placed on glass.

Ethics statement. All experiments using live animals were in compliance with animal welfare ethical regulations and approved by the Institute Animal Care and Use Committee before experimentation.

B16 melanoma *in vivo* models. Six–eight-week-old female C57BL/6 mice were purchased from Charles River Laboratories for Animal Experiment. Primary localized tumours were established by subcutaneously injecting B16F0 cells (range 250–10^6) grown on patterned gels, non-patterned gels (NP) or glass into the right lateral flank (the information of the number of mice in each experiment is described in each figure). Macroscopic tumour growth was serially measured (maximal length and width) with callipers three times a week. Tumour growth was checked every three days and experiments were stopped when the first mouse of the respective series had a tumour exceeding 2,000 mm^3. The volume of tumour was calculated using $V = (L \times W^2)/2$, where L is length and W is width. Experimental metastases were established by injecting 2.5×10^5 (B16F0 grown on pattern/glass or B16F10 grown on glass) or 3.0×10^4 (B16F0 grown on pattern/NP/glass) melanoma cells via lateral tail vein injection. Mice were either euthanized 5, 10, and 16 days (2.5×10^5 cells injected) post injection and used to quantify percentage tumour surface area within the lung parenchyma, or followed for survival analysis. Mice were used for determination of primary tumorigenesis and experimental metastases. No animals or target organ samples (lung tissue)

were excluded from analysis. Criteria used for primary tumorigenesis was the formation of subcutaneous tumours which were detectable by visual examination and measurable with callipers. For comparison of primary tumour formation kinetics, mice were evaluated daily until primary tumours exceeded 20 mm in diameter, then humanely euthanized. In some experiments evaluating primary tumorigenesis, study endpoints were dichotomous in nature, being either tumour formation or no tumour formation after a cumulative lapse of time (60 days). For experimental metastases, the primary endpoint was survival time, and mice were monitored daily until reaching criteria for humane euthanasia. Mice were used for determination of primary tumorigenesis and experimental metastases. Inoculation of mice with melanoma cells grown on different conditions (glass, non-pattern, and pattern) and different cell densities was not performed in a random fashion. Rather, cohorts of mice were predetermined to receive injections of melanoma cells grown under specified conditions and cell densities before inoculation. No blinding was done for these animal studies.

Ki67 immunohistochemistry. Five representative lung sections fixed in 10% formalin per mouse were immunohistochemically stained for Ki67. Within each lung section, three randomly selected parenchymal areas completely effaced by melanoma cells were microscopically quantified for Ki67 nuclear positivity and expressed as a percentage using ImageJ software.

Microscopy data analysis. Immunofluorescence images were analysed using ImageJ software. Multiple cells (over 20 patterns) were imaged for each condition and fluorescence intensities of single cells in patterns (after background subtraction) were used to compare marker expression. For cell curvature analysis, the number of cells in circular patterns (over 20 patterns) with different areas (3,000–100,000 μm^2) were counted, and cell curvature length was calculated based on the length of pattern perimeter and the number of cells at the perimeter. Average curvature angle and intensity of cells at the perimeter of the patterns were measured and plotted. For inhibition studies, positive cells which were above the maximum intensities of the glass control (ImageJ threshold) were counted, and the numbers were divided by total cells in patterns. For generating immunofluorescence heatmaps, cells cultured on various shapes were imaged on the same day using the same microscope and camera settings. Background intensities of raw fluorescent images were subtracted, and patterns were aligned in ImageJ with the same orientation as cultured across the surface, incorporated into a Z stack and the average intensity calculated for heatmap generation.

For segmentation analysis, cells cultured on each shape in a single monolayer were manually segmented for at least 100 single cells through immunostaining using ImageJ. Because cells predominantly express surface markers at the surface and not within nuclei and junctions, it is possible to segment single cells at the perimeter (line, convex, or concave): we used ×20 immunofluorescence images in ImageJ; the contrast and brightness were controlled to optimize the image for segmentation analysis; the surface region of each single cell at the perimeter was selected, excluding nuclei; the original image was re-opened, and the marker intensity of segmented single cells was measured using ImageJ; the background intensity was subtracted from the measured intensity values.

RNA isolation for microarray experiments. Adherent B16F0 and B16F10 cells cultured for five days on spiral patterns, non-patterned gels, or glass were lysed directly in Trizol reagent (Invitrogen) according to the vendor's instructions. Total RNA from each sample (12 duplicates) was extracted and quantified by photospectrometry using a NanoDrop ND-1000 (ThermoFisher). RNA quality was confirmed by an Agilent Bioanalyzer, and gene expression profiling performed using Illumina iScan Sentrix BeachChip technology at the Roy J. Carver Biotechnology Center at the University of Illinois at Urbana-Champaign using standard Illumina protocols (http://support.illumina.com/content/dam/illumina-support/documents/myillumina/3466bf71-78bd-4842-8bfc-393a45d11874/wggex_direct_hybridization_assay_guide_11322355_a.pdf). Illumina gene array data was pre-processed using GenePattern[38]. The background values were subtracted and thresholded. The data was then normalized using the quantile method. Heatmaps of fold changes over glass in gene expression were visualized using the Gene-E (http://www.broadinstitute.org/cancer/software/GENE-E) software package. A panel of metastasis genes was selected from a previous report by Clark and colleagues[39]. For finding relevant pathways, genes upregulated in patterns compared to glass were tested in the Database for Annotation, Visualization and Integrated Discovery (DAVID) website (http://david.abcc.ncifcrf.gov) and genes in each pathway were selected based on DAVID, and genes with negligible expression (below ten) were not included in the analysis.

Percentage tumour surface area. Five representative lung sections fixed in 10% formalin per mouse were microscopically examined at two different tissue planes separated by 50 μm. Subgross images (×1.25), including one image containing an embedded micrometer, were captured for each lung section at both tissue planes using standard microscopy imaging equipment. Images were imported into Adobe Photoshop Creative Cloud 2014 and the embedded micrometer was used to set a measurement scale of image pixels to length in mm (1,503 pixels = 5.0 mm). The parenchymal surface area of each lung lobe was subsequently measured using the Quick Selection Tool. Regions of B16 melanoma growth were then identified visually and cross-referenced with the histologic slide if necessary, surface area measured using the Magic Wand Tool, summed, and then expressed as a percentage relative to total parenchymal surface area using ImageJ software.

Modelling of cell monolayer. Abaqus software was used to construct and analyse a finite element model of contractile cell monolayers as described previously[14]. Briefly, the desired geometry was modelled in two layers: an active 20-μm-thick top layer and a passive 5-μm-thick bottom layer that is constrained at the bottom surface. The active layer is made to contract isotropically by applying a 5 K temperature drop. The von Mises stress at the bottom surface is reported. We confirmed convergence by testing multiple mesh sizes and layer properties.

Statistical analysis. Data was obtained from three independent experiments and expressed as the mean ± standard deviation (s.d.) unless otherwise specified. Statistical comparisons between two groups were based on Student's *t*-test and comparisons of more than two groups were performed by analysis of variance (ANOVA) with Tukey HSD Post-hoc testing to correct for multiple comparisons. Differences were considered significant at $P < 0.05$.

References

32. Tse, J. R. & Engler, A. J. Preparation of hydrogel substrates with tunable mechanical properties. *Curr. Protoc. Cell Biol.* **47,** 10.16.1–10.16.16 (2010).
33. Damljanović, V., Lagerholm, B. C. & Jacobson, K. Bulk and micropatterned conjugation of extracellular matrix proteins to characterized polyacrylamide substrates for cell mechanotransduction assays. *Biotechniques* **39,** 847–851 (2005).
34. Chang, C.-W., van Spreeuwel, A., Zhang, C. & Varghese, S. PEG/clay nanocomposite hydrogel: a mechanically robust tissue engineering scaffold. *Soft Matter* **6,** 5157–5164 (2010).
35. Miller, J. S. *et al*. Bioactive hydrogels made from step-growth derived PEG-peptide macromers. *Biomaterials* **31,** 3736–3743 (2010).
36. Schneider, C. A., Rasband, W. S. & Eliceiri, K. W. NIH Image to ImageJ: 25 years of image analysis. *Nature Methods* **9,** 671–675 (2012).
37. Zhang, D. & Kilian, K. A. The effect of mesenchymal stem cell shape on the maintenance of multipotency. *Biomaterials* **34,** 3962–3969 (2013).
38. Reich, M. *et al*. GenePattern 2.0. *Nature Genet.* **38,** 500–501 (2006).
39. Clark, E. A., Golub, T. R., Lander, E. S. & Hynes, R. O. Genomic analysis of metastasis reveals an essential role for RhoC. *Nature* **406,** 30–33 (2000).